COMPUTER-AIDED DESIGN & APPLICATIONS, 2017
VOL. 14, NO. 4, 392–407
http://dx.doi.org/10.1080/16864360.2016.1257183

Towards quantitative mesh pre-optimization for finite element analysis

Jean-Christophe Cuillière and Vincent Francois

Université du Québec à Trois-Rivières, Canada

ABSTRACT

In a previous research work, we introduced the concept of automatic mesh pre-optimization, also referred to as a priori mesh adaptation. Indeed, the basic idea underlying mesh pre-optimization is providing finite element analysis with meshes that have been adapted before analysis itself. It consists in automatically deriving mesh sizing functions from geometric features of the analysis domain. This allows providing the analyst with meshes that feature a certain degree of adaptation around sensitive zones or sensitive shapes (high curvature zones, narrow regions, sources of stress concentration, etc.) before any analysis, which also means before any a posteriori mesh adaptation. So far, mesh pre-optimization could not be considered as a quantitative adaptation since it does not explicitly target accuracy objectives, contrary to a posteriori mesh adaptation methods. This paper brings about new concepts in mesh pre-optimization that tend to make pre-optimization not only qualitative. It shows that, for 2D features, quantitative accuracy objectives in finite element analysis can reasonably be met, without using a posteriori adaptation. The approach proposed is applied in the context of plane stress analysis and it shows that user specified accuracy objectives can automatically be achieved at stress concentration locations. This improvement of mesh pre-optimization should not be regarded as an alternative to a posteriori adaptation but as an efficient way to obtain accurate preliminary FEA results, which is particularly interesting when evaluating design scenarios.

KEYWORDS

A priori adaptation; mesh sizing; CAD/FEA integration

1. Introduction

Despite the development of many alternative analysis methods such as Element Free Galerkin Methods [4], Isogeometric analysis [12] and XFEM methods [3], Finite element analysis (FEA) [20] remains the most efficient and versatile tool for solving a majority of engineering problems. One of its most interesting features is that it is now very well integrated inside CAD/CAM packages, which makes it a key tool that is used by engineers at nearly every stage along the product development process. It also makes that it is used by more diverse actors along this process, from very skilled analysts to early stages designers and manufacturing people. In this context, an important effort has been put towards reducing time, efforts and skill required to produce analyses from CAD models. Meanwhile, a significant effort has also been put towards better controlling FEA accuracy. In this direction, the development of a posteriori FEA error estimation methods [11, 15, 22] is a cornerstone since it allows quantifying the order of magnitude and spatial distribution of FEA error and using this information to automatically adapt FEA meshes so that the distribution of FEA error remains under a user specified threshold [22]. This adaptation process, referred to as *a posteriori mesh adaptation*, has become a common and useful tool that is now integrated inside most CAD/CAM and analysis packages. When using a posteriori mesh adaptation, an initial coarse mesh is gradually adapted through several analysis and error estimation loops. At the end, the initial mesh is locally refined and de-refined so that the user specified level of accuracy is reached everywhere. This process is very powerful but its major drawback is that, since it is driven by error estimation, mesh refinement occurs in zones that do not need to be refined, such as around singularities and boundary conditions. Also, it appears that providing the a posteriori mesh adaptation loop with initial meshes that already feature appropriate element size and element quality distributions has a very significant and positive impact on the final result. This improves the accuracy of final results and decreases the number of adaptation loops. Providing the FEA with meshes that already feature mesh adaptation in some specific zones, before any analysis, is referred to as *a priori mesh adaptation* or *mesh pre-optimization* (where *pre* stands for before analysis). If compared to *a posteriori mesh adaptation*, a lot less research effort has been put towards a priori mesh adaptation. Indeed, even if a few approaches have been proposed in the

CONTACT Jean-Christophe Cuillière cuillier@uqtr.ca

literature [7, 13, 14, 16–19], it remains a very open field of investigation. This is mainly due to the fact that a priori mesh adaptation is extremely ambitious and complex in a general context. It involves automatically identifying features that are likely to affect FEA accuracy (for example geometric features that are source of stress concentration) and automatically applying appropriate mesh adaptation strategies around these features. This typically involves using feature identification techniques combined with knowledge synthesis, which are both complex to implement and highly sensitive to the analysis context. For example, in mechanical analysis, stress concentration not only depends on geometry but also on boundary conditions. As illustrated in Fig. 1, the same hole in the same part may be (Fig. 1a) or may not be (Fig. 1b) the source of stress concentration, depending on the way it is loaded.

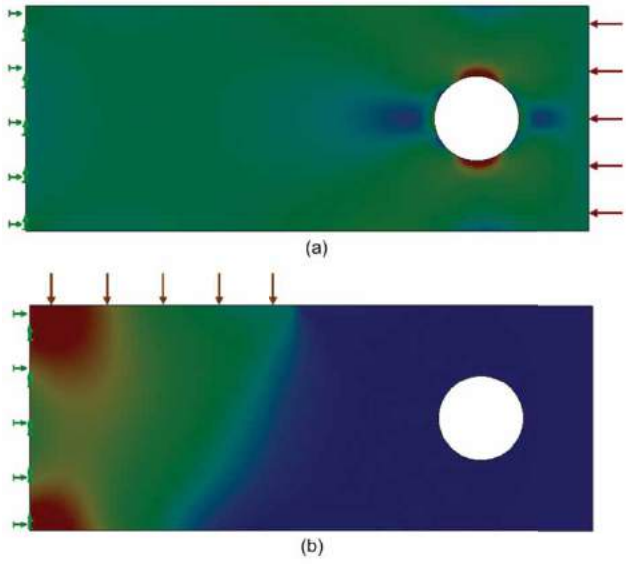

Figure 1. Influence of boundary conditions on stress concentration.

The fact that, at this point, all approaches to a priori mesh adaptation are qualitative is another major concern. Indeed, contrary to a posteriori adaptation, a priori mesh adaptation basically targets obtaining better FEA results than when using coarse meshes, without explicitly quantifying FEA accuracy objectives. We have shown in a previous paper [5] that a quantification of a priori adaptation can be foreseen, which means that a priori adaptation can reasonably meet a user specified degree of accuracy in FEA results. This first study was limited to a priori mesh adaptation around through holes in the context of plane stress analysis with linear triangular elements but the results obtained are very promising. Fig. 2 shows an example of results obtained on a sample case. Fig. 2a presents the sample case considered while Fig. 2b shows the triangular mesh obtained after a priori mesh adaptation (in this case the FEA accuracy objective δ_{target} is 10%). Fig. 2c shows the distribution of von Mises stress derived from this mesh and Fig. 2d finally illustrates a distribution of the "actual" FEA error

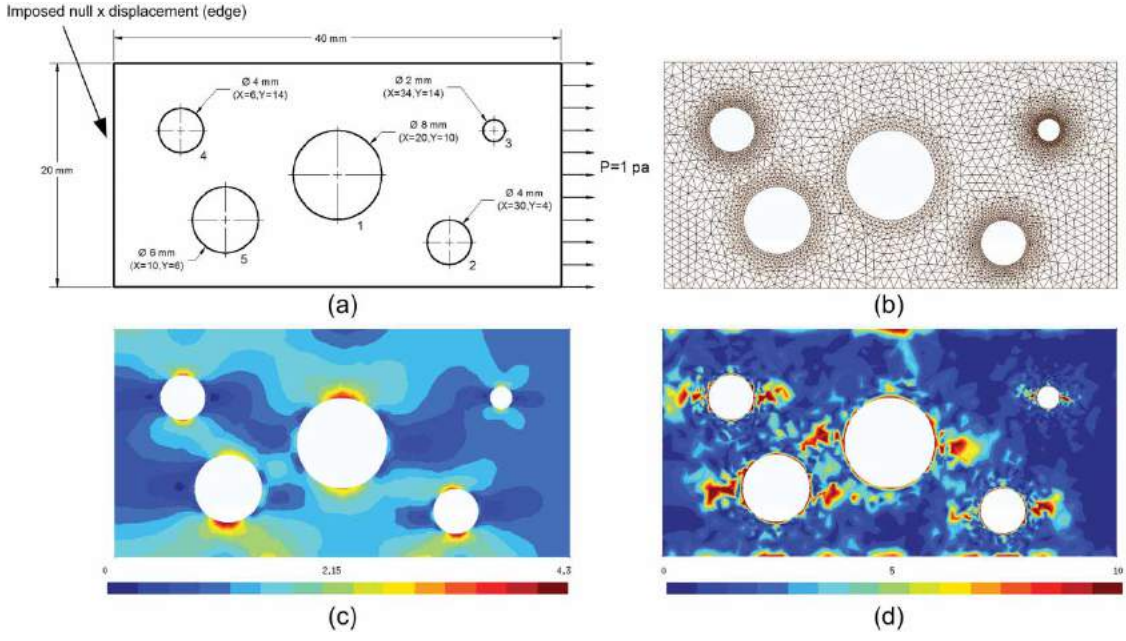

Figure 2. A priori mesh adaptation around holes and results derived (a) Geometry (b) Adapted mesh (c) Von Mises stress distribution (d) "Actual" error distribution (in %).

obtained with this mesh. This so called "actual" FEA error is obtained from a reference von Mises stress distribution $\tilde{\sigma}_{VM}(x,y)$ that is computed using an extremely refined quadratic mesh. Thus, $\tilde{\sigma}_{VM}(x,y)$ is assimilated to the exact solution and the "actual" FEA error $\delta(x,y)$ is calculated (in %) for a given FEA von Mises stress result $\sigma_{VM}(x,y)$ as:

$$\delta(x,y) = \left| \frac{\sigma_{VM}(x,y) - \tilde{\sigma}_{VM}(x,y)}{\tilde{\sigma}_{VM}(x,y)} \right| \quad (1)$$

The objective of this a priori mesh adaptation is that $\delta(x,y) \leq \delta_{\text{target}}$ at all stress concentration locations, which is quite well achieved as illustrated in Fig. 2d. Indeed, $\delta(x,y)$ values at stress concentration points around the 5 holes are between 8.8% and 10.9% for $\delta_{\text{target}} = 10\%$. Fig. 2d also shows that, out of these stress concentrations zones, $\delta(x,y)$ exceeds δ_{target}at some locations. However this is not a problem in practice since it always happens at locations where von Mises stress is very low.

These preliminary results show that a priori mesh adaptation around through holes, in the context of plane stress analysis, can actually be quantitative and not only qualitative. In this paper, we present an extension of this first approach to other types of features. The main objective of this paper is showing that the methodology presented in [5] also applies to notches and shoulders. This allows implementing a priori mesh adaptation for plane elasticity problems in a more general context, for which different types of features are mixed all together. This paper is organized as follows. In section 2, we start introducing core principles on which our approach towards quantitative mesh pre-optimization is based. In section 3 we present validation examples on cases with single features followed by cases mixing different types of features. The paper ends with a conclusion about perspectives of future work.

2. Towards quantifying mesh pre-optimization

2.1. Types of features considered

In this paper, as introduced above, we focus on controlling the FEA error around three types of features for planar elasticity FEA simulations (plane stress is considered here but similar results can be obtained for plane strain simulations). Note that plane problems are only considered here to lighten FEA models used in the investigation. Consequently, results obtained cannot be used as is in cases where 3D effects are not negligible. The three types of features considered (through holes, notches and shoulders) are source of stress concentration as illustrated in Fig. 3. It is worth mentioning that, in this work, the direction of loading and more generally boundary conditions (see Fig. 1) are not taken into account, which means that each feature considered will be the source of mesh adaptation in all cases. It is also important to underline that in this work, it is assumed that the type, location and parameters of all geometric features considered are known. The focus of this paper is indeed on a priori mesh adaptation itself and not on feature identification methods that are necessary to make the whole a priori adaptive process completely automatic.

2.2. Investigation on references cases

As presented with details in [5], the first basic principle underlying our mesh pre-optimization approach is finding, for each type of feature considered, a quantitative relationship between mesh sizing and FEA error for a reference case. The reference case considered for each type of feature is illustrated in Fig. 4.

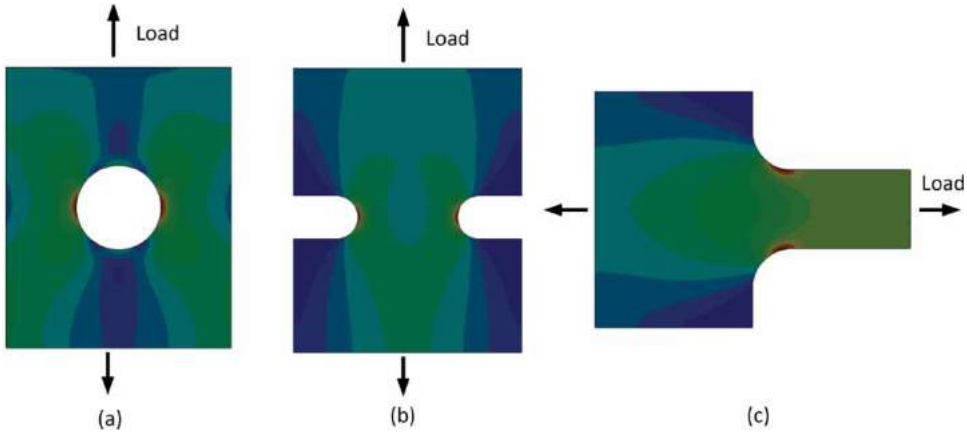

Figure 3. Three types of features (a) Through holes (b) Notches (c) Shoulders.

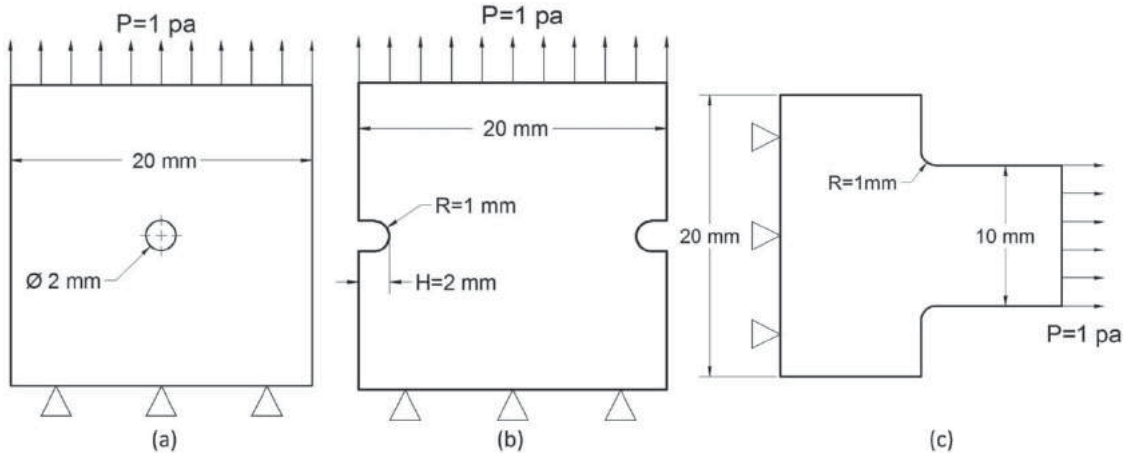

Figure 4. Three reference cases (a) Through hole (b) Notch (c) Shoulder.

On each of these reference cases, a first finite element analysis is performed using an extremely refined mesh with quadratic triangles. The FEA solution derived from these meshes is referred to, in this work, as a reference solution. In this paper, considering the dimensions used, all reference solutions are computed using meshes with 0.025 mm quadratic triangles. Also, FEA models used for all these analyses only considers half the plate due to symmetry, as shown in Fig. 5. Von Mises stress solutions (as shown in Fig. 5) derived from these quadratic meshes are considered as close enough to the exact solutions and they are noted $\tilde{\sigma}_{VM}(x, y)$. For each reference case, at the stress concentration location (x_c, y_c) we have $\tilde{\sigma}_{VM}(x_c, y_c) = \tilde{\sigma}^{ref}_{VM}$. Then, sets of finite element analyses are performed, on these reference cases, using meshes with constant size $E(x, y) = E$ and linear triangular elements. For each value of E a new FEA stress distribution $\sigma_{VM}(x, y)$ is obtained and its value at the stress concentration location is $E\delta_{ZZ}(x, y)$ $\sigma_{VM}(x_c, y_c) = \sigma^{ref}_{VM}$.

From $\tilde{\sigma}_{VM}(x, y)$ and $\sigma_{VM}(x, y)$ distributions, we can compute the distribution of the (so-called) "actual" error $\delta(x, y)$ as introduced in the previous section (see Fig. 6a b and c). A different distribution $\delta(x, y)$ is obtained for each element size used. $\delta(x, y)$ around each feature of reference cases is illustrated in Fig. 6 for $E = 0.15$ mm and it is compared with the error as estimated using the Zhu-Zienkiewicz [21] classical estimator $\delta_{ZZ}(x, y)$. In this comparison, the same color scale is used (between 0 and 12%). Of course these two error distributions cannot be compared quantitatively since they are based on completely different principles. Moreover, is constant per

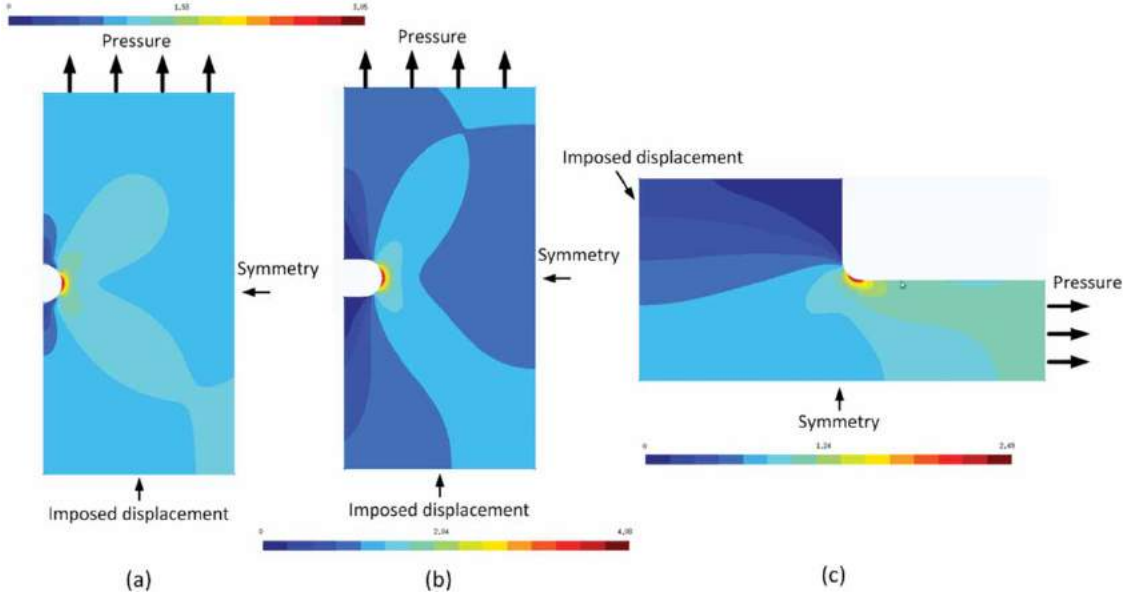

Figure 5. FEA models and reference von Mises stress distributions $\tilde{\sigma}_{VM}(x, y)$ for reference cases (a) Through hole (b) Notch (c) Shoulder.

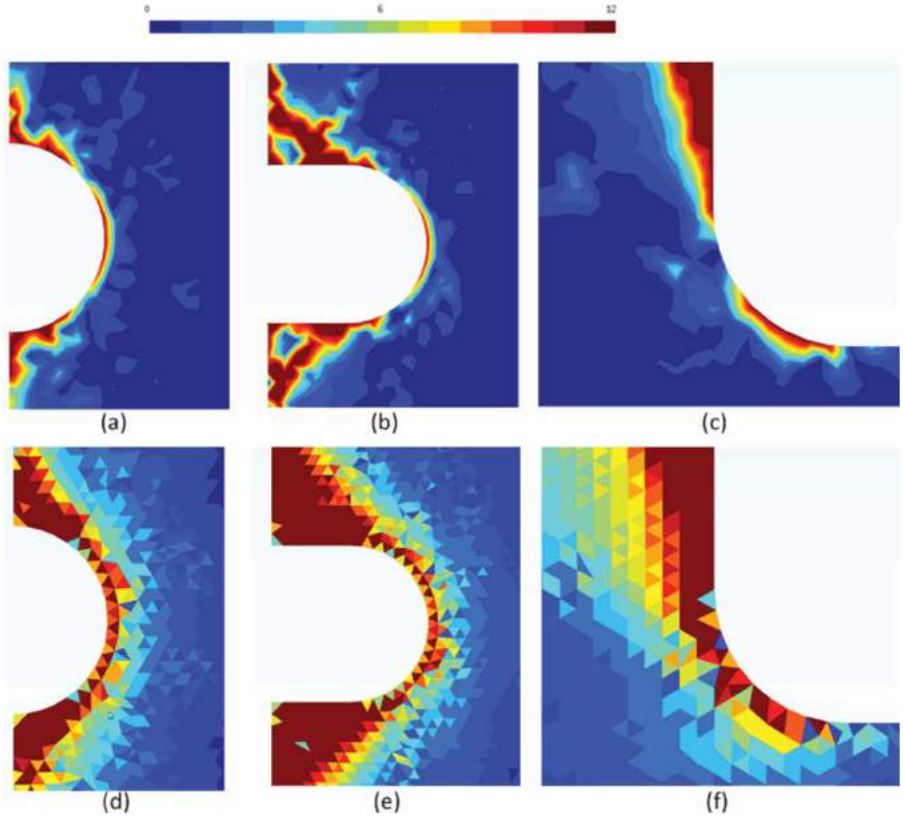

Figure 6. $\delta(x,y)$ (a) (b) (c) and $\delta_{ZZ}(x,y)$ (d) (e) (f) for $E = 0.15$ mm.

element, which is not the case for $\delta(x,y)$. However, the interesting aspect of this comparison is that these two error distributions are similar and that, for both distributions, the maximum error zone is not located at concentration points but in very low stress zones.

Once computed "actual" error distributions for different values of element size E, we assessed the relationship between E and the actual error at stress concentration, noted $\delta^{ref} = \delta(x_c, y_c)$. Quite surprisingly, we found that $\delta^{ref} = F(E)$ is linear for the three types of features (see Fig. 7), which is extremely interesting and, as shown in the next paragraphs, which opens the door to quantifying a priori mesh adaptation.

Note that $E$is taken between $E = 0.05$ mm and $E = 0.3$ mm. Indeed, for $E > 0.3$ mm FEA results are not representative because element size is too close to the radius of reference features ($R = 1$ mm). For $E < 0.05$ mm, results are not representative either because E comes too close to element size used for the reference quadratic solution ($E = 0.025$ mm in this work).

We also showed in [5] that element arrangement and element quality has a very important impact on linearity

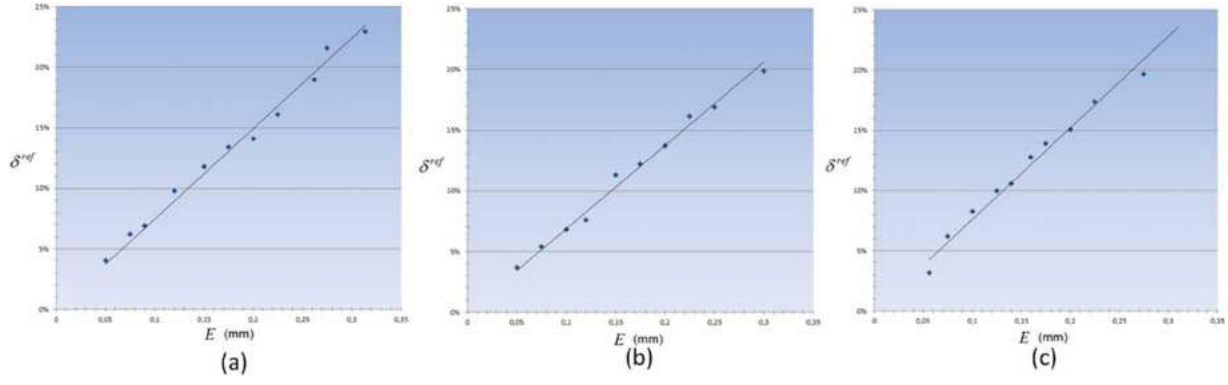

Figure 7. Linearity between δ^{ref} and E for the three reference cases (a) Through hole (b) Notch (c) Shoulder.

between δ^{ref} and E. Indeed, it appears that for good element arrangements and good element quality (elements with a shape that is as close as possible to an equilateral triangle) linearity between δ^{ref} and $E$is nearly perfect. Another interesting aspect of our investigation on reference cases is that we found that the evolution of δ along x axis (as defined in [5]) from the stress concentration point also varies linearly with von Mises stress second derivative $\frac{\partial^2\tilde{\sigma}_{VM}}{\partial x^2}$.

Moreover, after investigating reference cases (with $R = 1$ mm) we found that they can be extrapolated to other radii using a simple proportional law. It appears indeed that, for two cases with the same fraction $\frac{E}{R}$, δat concentration point is very close if there are no side effects. Side effects are well known and can indeed be observed if a hole radius for example is not small enough if compared to the plate width.

2.3. A new approach to automatic mesh pre-optimization

2.3.1. Automatic mesh pre-optimization around the three types of features

These three observations (linearity between δ^{ref} and E, linearity between $\delta(x)$ and $\frac{\partial^2\tilde{\sigma}_{VM}}{\partial x^2}$ and linearity with radius) can then be extrapolated to derive sizing functions around these three types of features that allow targeting quantitative FEA accuracy at concentration points for any radius. However, mesh sizing functions constrained by requirements related to element quality. In general, setting up good a priori mesh sizing functions relies on making a compromise between element size and element shape. The ideal triangular shape for obtaining the most accurate FEA results is generally equilateral but this comes in contradiction with mesh size variation. Different approaches can be used to make the best compromise between size and shape. One efficient and easy way to handle this problem is applying a threshold on the size map gradient $\|\vec{\nabla}E(x,y)\|$, which is the solution used in this work. We investigated different solutions to take all these constraints into account, among which using non-linear sizing functions based on $\frac{\partial^2\tilde{\sigma}_{VM}}{\partial x^2}$mixed with a threshold on $\|\vec{\nabla}E(x,y)\|$ (see [5] for more details). After many tests, we finally came to the conclusion that accurate results can be achieved using a more simple approach, based on linear sizing functions mixed with influence zones. We introduced the concept of influence zones in a previous work about qualitative mesh pre-optimization [7]. This basically consists in assuming that the major influence of a given stress concentration feature $A_i$on FEA results is confined inside a zone surrounding this feature. From this assumption, mesh sizing functions are built over simulation domains based on the following principles:

- Outside all influence zones, the mesh sizing function is constant: $E(x,y) = E_g$
- Inside an influence zone A_i, $E(x,y)$ linearly increases with distance d to the feature associated with the influence zone. This variation is noted $E_i(d)$.
- Since $E_i(d)$ is linear while $\frac{\partial^2\tilde{\sigma}_{VM}}{\partial x^2}$is not, an averaging coefficient is applied.
- At locations where several influence zones overlap, a compromise must be made between these influence zones.
- $E(x,y)$ must be continuous and smooth enough to avoid bad element quality.

In this work, the influence zone of a given feature A_i with radius R_i is defined as the set of points that are closer to the feature than an influence distance (or scope) Δ_i. This makes that influence zones associated with the three types of stress concentration features considered (holes, notches and shoulders) are defined as illustrated in Fig. 8.

Inside the influence zone of a given feature A_i (with radius R_i), $E_i(d)$ the mesh sizing function at distance d toA_i is defined based on the accuracy target δ_{target}, on R_i, and on linear variations obtained in Fig. 7.

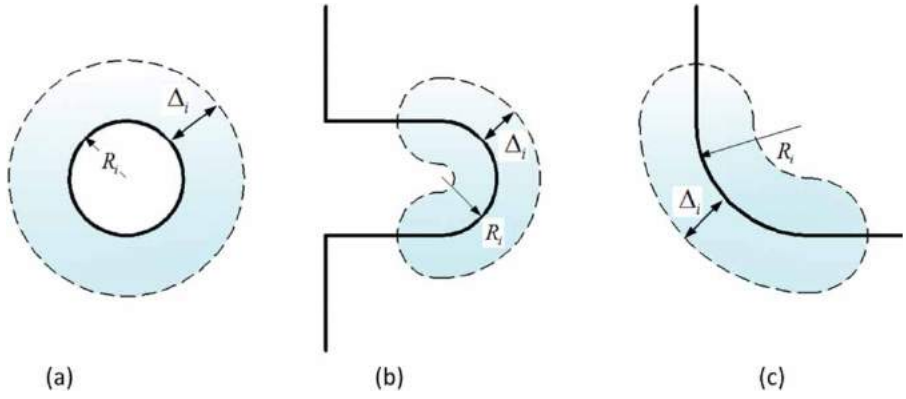

Figure 8. Influence zones for the three types of features.

For reasons introduced above, keeping the gradient $\|\vec{\nabla}E(x,y)\|$ under a threshold allows ensuring that the transition between lower element size and higher element size is smooth enough so that it has a limited effect on element quality. After many experiments, we came to imposing $\|\vec{\nabla}E(x,y)\| = \frac{1}{4}$ inside of all influence zones, which imposes the slope of $E_i(d)$ since it is linear. It is also worth noting that.in this work, the accuracy targetδ_{target} is the same for all features in a part, which means that if $\delta_{\text{target}} = 10\%$ for example, we target that the "actual" FEA error $\delta(x,y)$(see equation 1) should not exceed 10% at any stress concentration locations in the part.

Thus, $E_i(d)$ is practically defined as:

$$E_i(d) = \frac{1}{4}.d + \alpha.R_i.\delta_{\text{target}} \text{ for } d \leq \Delta_i$$
$$E_i(d) = E_g \text{ for } d \geq \Delta_i \quad (2)$$

with $\Delta_i = 4.(E_g - \alpha.R_i.\delta_{\text{target}})$ Thus, the two principles on which the variation of mesh size around a given feature A_i is based are

- Mesh size is $E_i(0) = \alpha.R_i.\delta_{\text{target}}$ on the feature
- Mesh size increases linearly with a $\frac{1}{4}$ slope to reach $E_i(d) = E_g$at distance$d = \Delta_i$.

Since $E_i(0)$ and Δ_i vary with R_i, they are different for each feature. Parameter α is calculated from the linear relations obtained for each type of feature in Fig. 7. A close look at Fig. 7 shows that parameterα is slightly different for each type of feature. Consequently, we could have considered a different α for each type of feature. However, since αvalues are close enough, we considered the same value $\alpha = 0.875$ for the three types of features. Of course, this choice is based on considering the worst case. Outside influence zones of features, mesh size is constant and equal to E_g. The computation of E_g is automatic and it is taken as the mean value of element size specification at distance R_i from each feature. Thus, for a part with N features A_i, E_g is automatically calculated as:

$$E_g = \frac{1}{N}.\sum_{i=1}^{N}\left(\frac{1}{4}.R_i + \alpha.R_i.\delta_{\text{target}}\right) \quad (3)$$

2.3.2. Automatic mesh pre-optimization for 2D parts in general

Given a 2D part and an accuracy target δ_{target}, mesh pre-optimization is fully automated:

- *Step1:* Features A_i and associated radii $R_i(i = 1 \ldots N)$ are first automatically identified on the geometric model, which is quite simple since we consider 2D parts.
- *Step 2:* Mesh size outside influence zones E_g is calculated from equation 3
- *Step 3:* Scope of influence zones Δ_i and mesh size variation $E_i(d)$ inside each influence zone are calculated from equation 2. At any location where two (or more) influence zones overlap, the minimum size provided by overlapping mesh size specifications is considered.

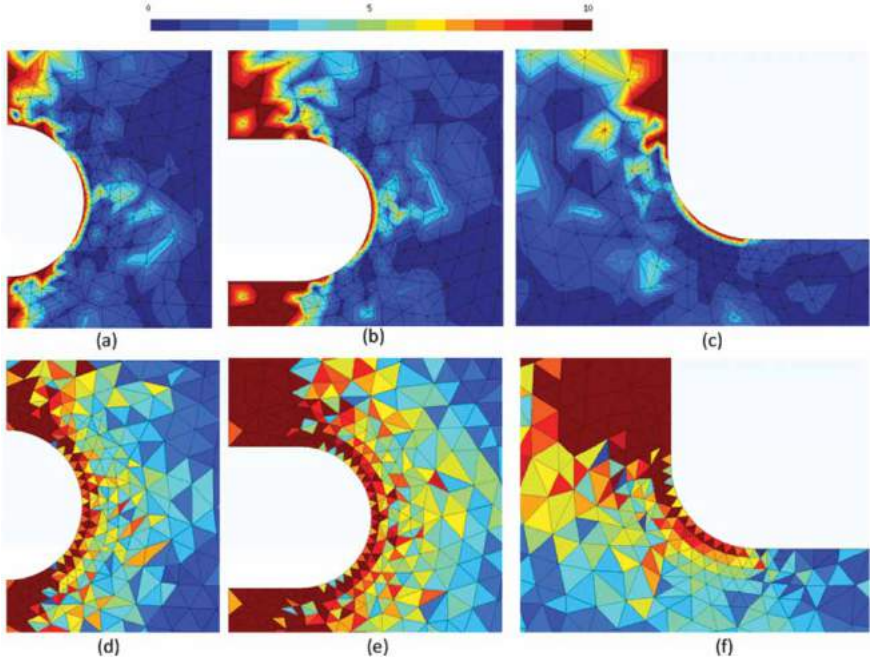

Figure 9. $\delta(x,y)$ (a) (b) (c) and $\delta_{ZZ}(x,y)$ (d) (e) (f) for $\delta_{\text{target}} = 10\%$.

- *Step 4:* The size map is stored across the whole part using a background grid (see reference [5])
- *Step 5:* Automatic mesh generation is performed based on the size map

3. Pre-optimization validation tests

3.1. Implementation

The proposed method is implemented in a Linux based CAD-FEA research platform developed by our team [6, 8, 9]. This platform integrates 3D modeling, analysis and topology optimization capabilities. It is based on C++ code, on Open Cascade^{TM} libraries [2] and on the use of Code_Aster^{TM} [1] as FEA solver. In this paper we use Gmsh^{TM} [10] for visualizing meshes, size maps, FEA results and error distributions.

3.2. Results for the three reference cases

The a priori mesh adaptation strategy described in the previous section is first applied on the three reference cases. Fig. 9 first illustrates distributions of the "actual" and estimated errors $\delta(x,y)$ and $\delta_{ZZ}(x,y)$ for $\delta_{\text{target}} = 10\%$.

Here again, it clearly appears that the "actual" FEA error $\delta(x,y)$ is around δ_{target}at stress concentration locations and that both errors are maximum in zones

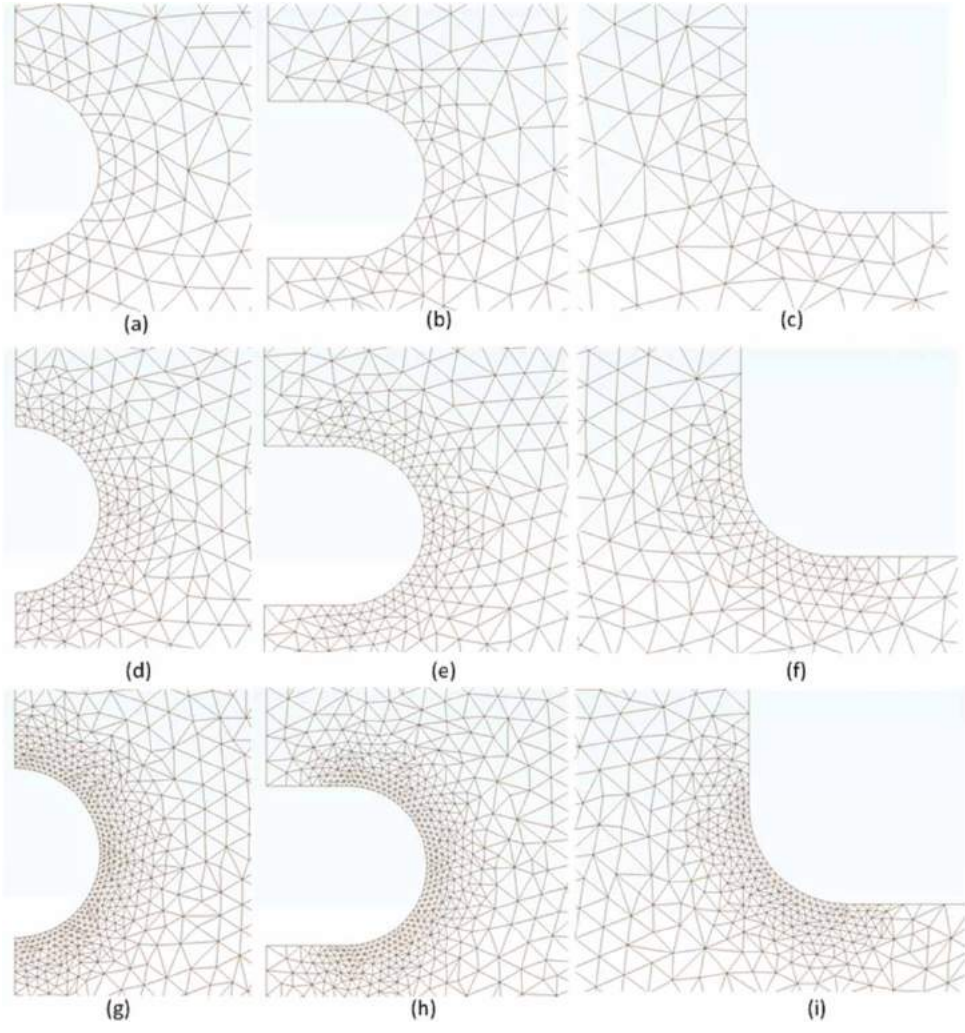

Figure 10. Results on reference cases for $\delta_{\text{target}} = 5\%$, 10% and 20%.

Table 1. Synthesis of results after pre-optimization at stress concentration points for reference cases.

	$\tilde{\sigma}_{VM}(x_c,y_c)$	$\delta(x_c,y_c)$ $\delta_{\text{target}} = 3\%$	$\delta(x_c,y_c)$ $\delta_{\text{target}} = 5\%$	$\delta(x_c,y_c)$ $\delta_{\text{target}} = 10\%$	$\delta(x_c,y_c)$ $\delta_{\text{target}} = 20\%$
Hole (R = 1 mm)	*3,05 Pa*	*1,6%*	*4,3%*	*8,5%*	*15,4%*
Notch (R = 1 mm, H = 2 mm)	*4,08 Pa*	*2,5%*	*3,9%*	*7,6%*	*14,7%*
Shoulder (R = 1 mm)	*2,49 Pa*	*3,2%*	*5,4%*	*10,5%*	*18,8%*

where von Mises stress is very low. Then, Fig. 10 shows meshes obtained after a priori mesh adaptation for three accuracy objectives (5%, 10% and 20%) and Tab. 1 summarizes results for the "actual" FEA error at stress concentration points $\delta(x_c, y_c)$ for these three objectives. It appears that the accuracy targetδ_{target} is met in general even if $\delta(x_c, y_c)$ is slightly over the objective for the shoulder in three cases. This shows that, using the approach as presented in section 2.3, pre-optimization is not only qualitative and that quantitative accuracy targets can reasonably be met at stress concentration locations.

3.3. Results for single features

3.3.1. A first set of results with single features

Our a priori mesh adaptation strategy is then applied on single features for which geometric parameters (radii for holes and shoulders and radius/length for notches) are modified from reference cases. In these cases, plate length and width along with boundary conditions are kept the same. Thus the only modification is applied on dimensions of features themselves. The three features considered below are a hole with $R = 2$ mm, a notch with $R = 2$ mm and $H = 4$ mm and a shoulder with $R = 2$ mm. Fig. 11 presents reference von Mises stress distributions along with pre-optimized meshes and FEA errors ($\delta(x, y)$ and $\delta_{ZZ}(x, y)$) with accuracy objective $\delta_{\text{target}} = 10\%$ for the three cases. The color scale considered for Fig. 11c and Fig. 11d is 0–10%. For Fig. 11a the color scale varies since maximum reference von Mises stress is different for each feature as shown in Tab. 2. Tab. 2 also summarizes for the "actual" FEA error at stress concentration points$\delta(x_c, y_c)$for these three cases with various accuracy objectives. These results confirm that accuracy targets can reasonably be met at stress concentration locations.

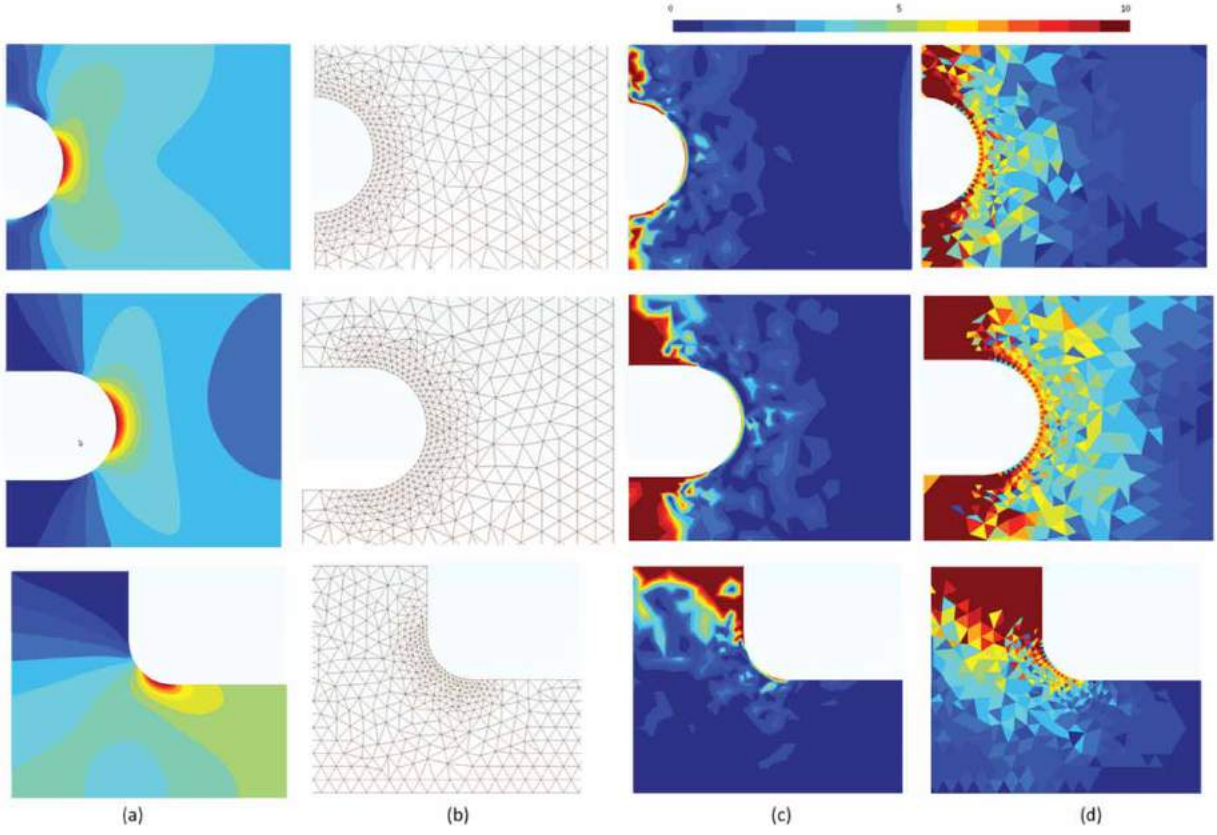

Figure 11. Results for R = 2 mm (and H = 4 mm for the notch) and $\delta_{\text{target}} = 10\%$ (a) Reference stress distribution $\tilde{\sigma}_{VM}(x, y)$ (b) Pre-optimized mesh (c) $\delta(x, y)$ (d) $\delta_{ZZ}(x, y)$.

Table 2. Synthesis of results after pre-optimization at stress concentration points for other feature dimensions.

	$\tilde{\sigma}_{VM}(x_c, y_c)$	$\delta(x_c, y_c)$ $\delta_{\text{target}} = 3\%$	$\delta(x_c, y_c)$ $\delta_{\text{target}} = 5\%$	$\delta(x_c, y_c)$ $\delta_{\text{target}} = 10\%$	$\delta(x_c, y_c)$ $\delta_{\text{target}} = 20\%$
Hole (R = 2 mm)	*3,22 Pa*	*0,9%*	*4,3%*	*8,7%*	*11,2%*
Notch (R = 2 mm, H = 4 mm)	*4,29 Pa*	*2,6%*	*3,7%*	*7,8%*	*14,1%*
Shoulder (R = 2 mm)	*1,98 Pa*	*3,1%*	*4,6%*	*9,1%*	*15,6%*

3.3.2. A second set of results for various notch parameters

In the next example pre-optimization is applied to notches with different ratio $\frac{H}{R}$. $H = 3$ mm for the first case, $H = 4$ mm for the second case, $R = 1$ mm $H = 5$ mm for the third case and $H = 5$ mm for the fourth case. Like in previous cases, $\delta_{\text{target}} = 10\%$ has been considered as accuracy target. Reference von Mises stress distributions, pre-optimized meshes and FEA errors ($\delta(x, y)$ and $\delta_{ZZ}(x, y)$) are presented in Fig. 12 for these four new cases with a 0–10%. color scale for c and d. Here also, the color scale in Fig. 12a varies since maximum reference von Mises stress is different for each notch as shown in Tab. 3.

Results for the "actual" FEA error at stress concentration points $\delta(x_c, y_c)$ are summarized in Tab. 3. These results illustrate that accuracy target is met at stress concentration locations for all notch dimensions. This is due to the fact that, as mentioned in section 2.3, a unique parameter $\alpha = 0.875$ has been chosen for all types of features, based on a worst case logic, which makes that results are, in general, likely to be worse for shoulders and holes than for notches.

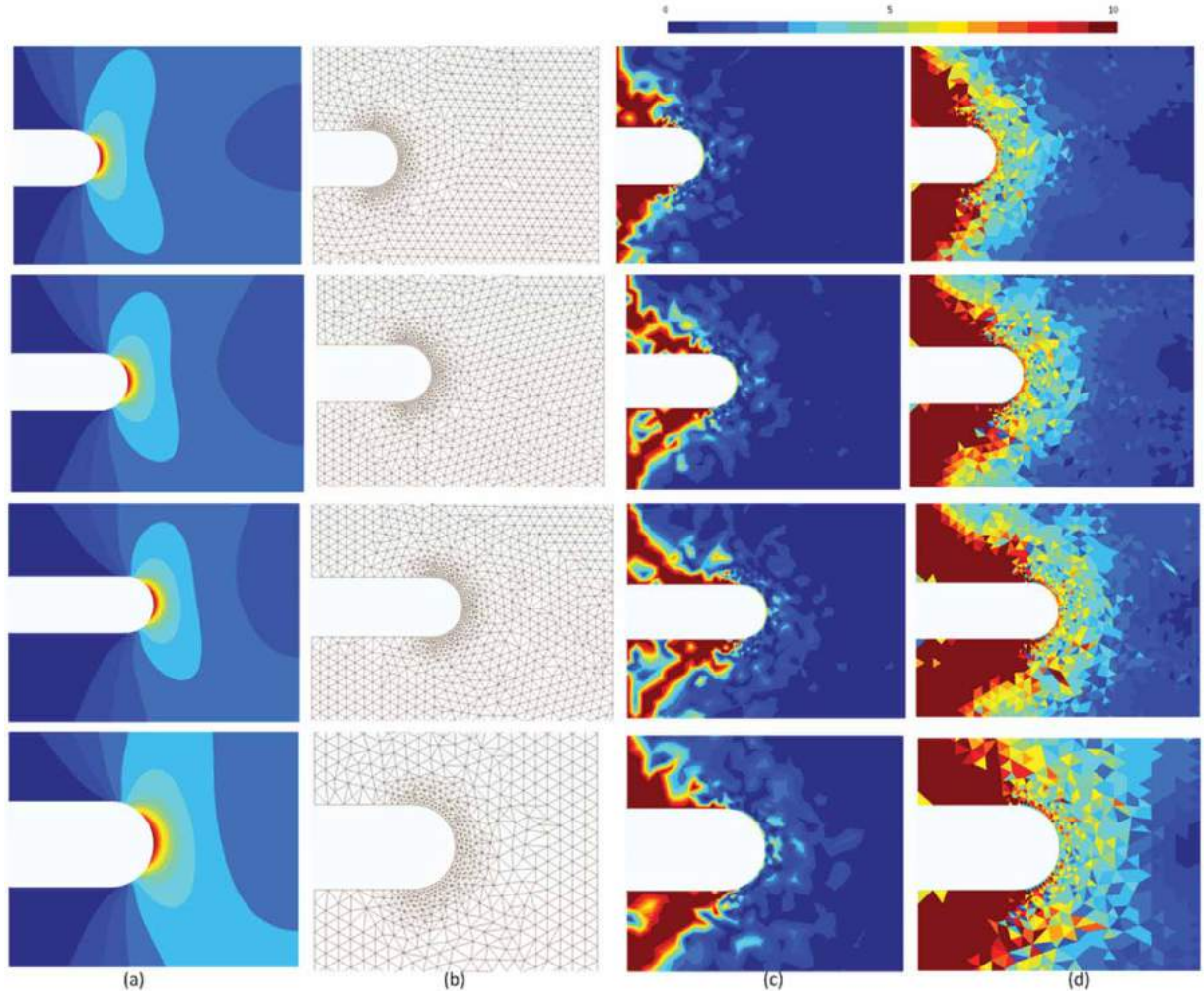

Figure 12. Results for various various notch $\frac{H}{R}$ ratio and $\delta_{\text{target}} = 10\%$.

Table 3. Synthesis of results after pre-optimization at stress concentration points for various notch $\frac{H}{R}$ ratio.

	$\tilde{\sigma}_{VM}(x_c, y_c)$	$\delta(x_c, y_c)$ $\delta_{\text{target}} = 3\%$	$\delta(x_c, y_c)$ $\delta_{\text{target}} = 5\%$	$\delta(x_c, y_c)$ $\delta_{\text{target}} = 10\%$	$\delta(x_c, y_c)$ $\delta_{\text{target}} = 20\%$
Notch (R = 1 mm, H = 3 mm)	*4,92 Pa*	*2,5%*	*3,7%*	*7,2%*	*13,7%*
Notch (R = 1 mm, H = 4 mm)	*5,71 Pa*	*2,5%*	*3,7%*	*7,2%*	*13,7%*
Notch (R = 1 mm, H = 5 mm)	*6,50 Pa*	*1,1%*	*3,5%*	*6,9%*	*13,2%*
Notch (R = 1.5 mm, H = 5 mm)	*5,46 Pa*	*2,4%*	*3,9%*	*4,7%*	*14,7%*

3.4. Results for multiple features

3.4.1. A first case with multiple features

We consider now a first case with the three types of features. Geometry is illustrated in Fig. 13 and it shows that the part features two notches, one shoulder and three holes with various radii. In this figure, features are numbered (between 1 and 6) for reference. Like for previous validation cases, a first finite element analysis is performed using an extremely refined mesh with quadratic triangles ($E = 0.025$ mm like in previous cases). The FEA model used for all analyses on this case along with the reference von Mises stress distribution $\tilde{\sigma}_{VM}(x, y)$ are shown in Fig. 14. In Fig. 14, the color scale is adjusted (between 0 and 8 Pa) so that all stress concentration zones can be seen.

Fig. 15a and Fig. 15b show meshes generated using the adaptation scheme proposed in this paper for respectively $\delta_{\text{target}} = 10\%$ and $\delta_{\text{target}} = 20\%$. Like in validation cases

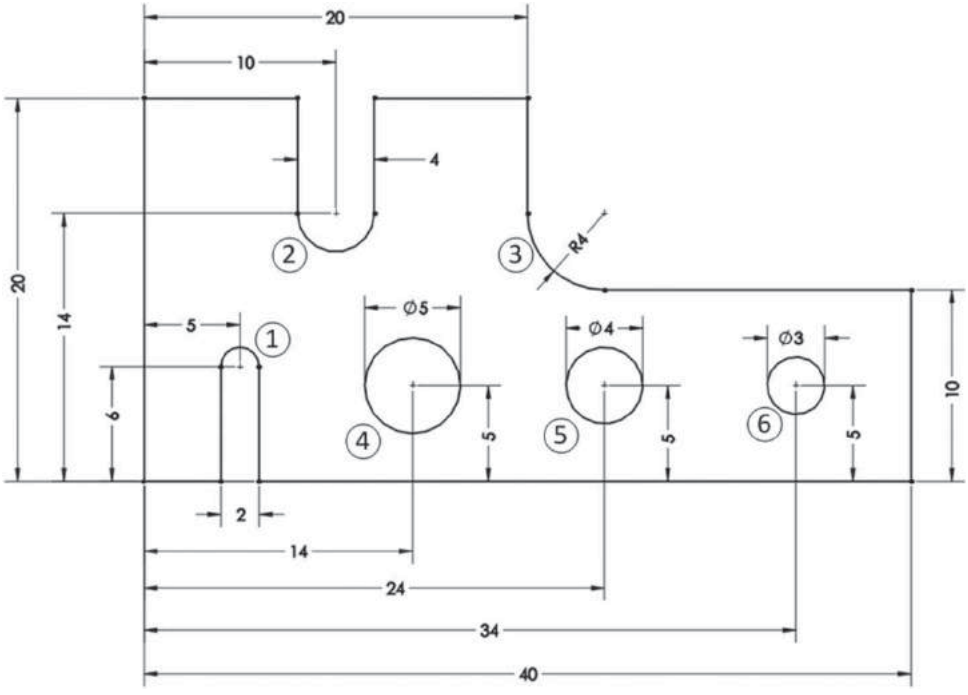

Figure 13. Geometry for the first case with multiple features.

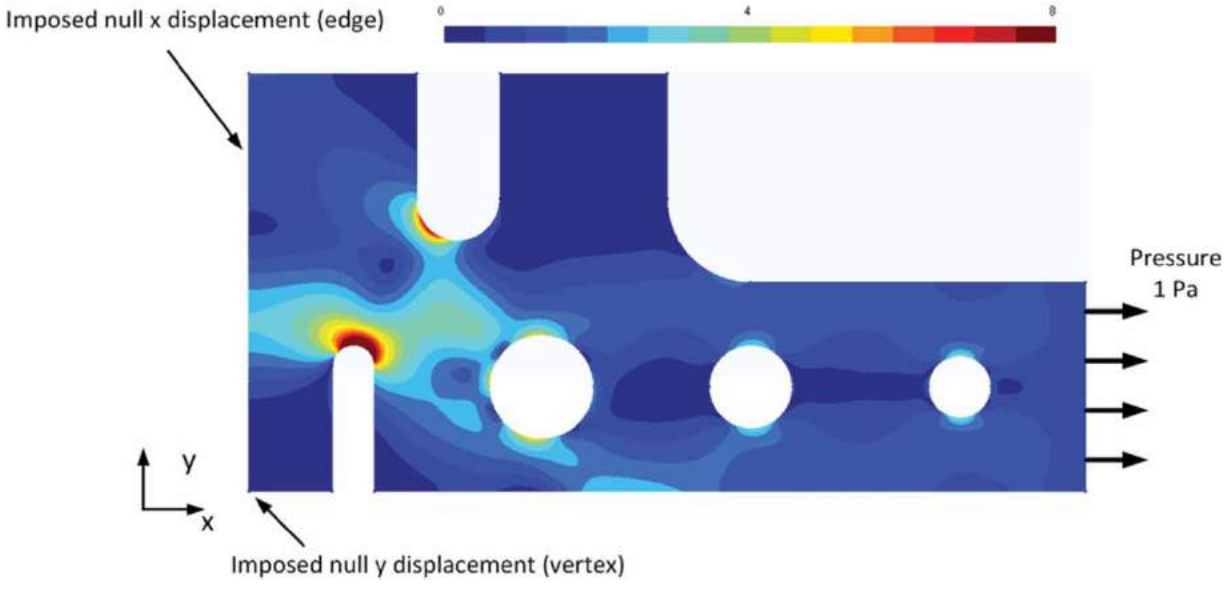

Figure 14. FEA model and reference von Mises stress $\tilde{\sigma}_{VM}(x, y)$ for the first case with multiple features.

with single features, distributions of actual (middle figures) and estimated (lower figures) FEA errors $\delta(x, y)$ and $\delta_{ZZ}(x, y)$ are shown for these two accuracy objectives in Fig. 15 (note that the color scale is adapted to accuracy objectives). A close look at stress concentration zones in Fig. 14 and at the two distributions of $\delta(x, y)$ in Fig. 15 globally show that accuracy objectives are met at stress concentration points and that maximum error occurs where von Mises stress is very low. The fact that accuracy objectives are globally met is confirmed by the synthesis of results presented in Tab. 4 where the "actual" FEA error at stress concentration points $\delta(x_c, y_c)$ is provided for each feature (from 1 to 6 as illustrated in Fig. 13). All these results confirm conclusions made in the previous section for single features. Indeed, even if the accuracy objective is slightly exceeded in some cases (results for which δ_{target} is exceeded by more than 10% are in red in Tab. 4), the general trend of results shows that using such a mesh sizing function allows "a priori" controlling the FEA error around stress concentration points for sets of features in general, which is very powerful and very promising. Tab. 4 shows that results globally tend to be worse for lower accuracy objectives, which can be explained by the fact that for lower accuracy objectives, the mesh size gets

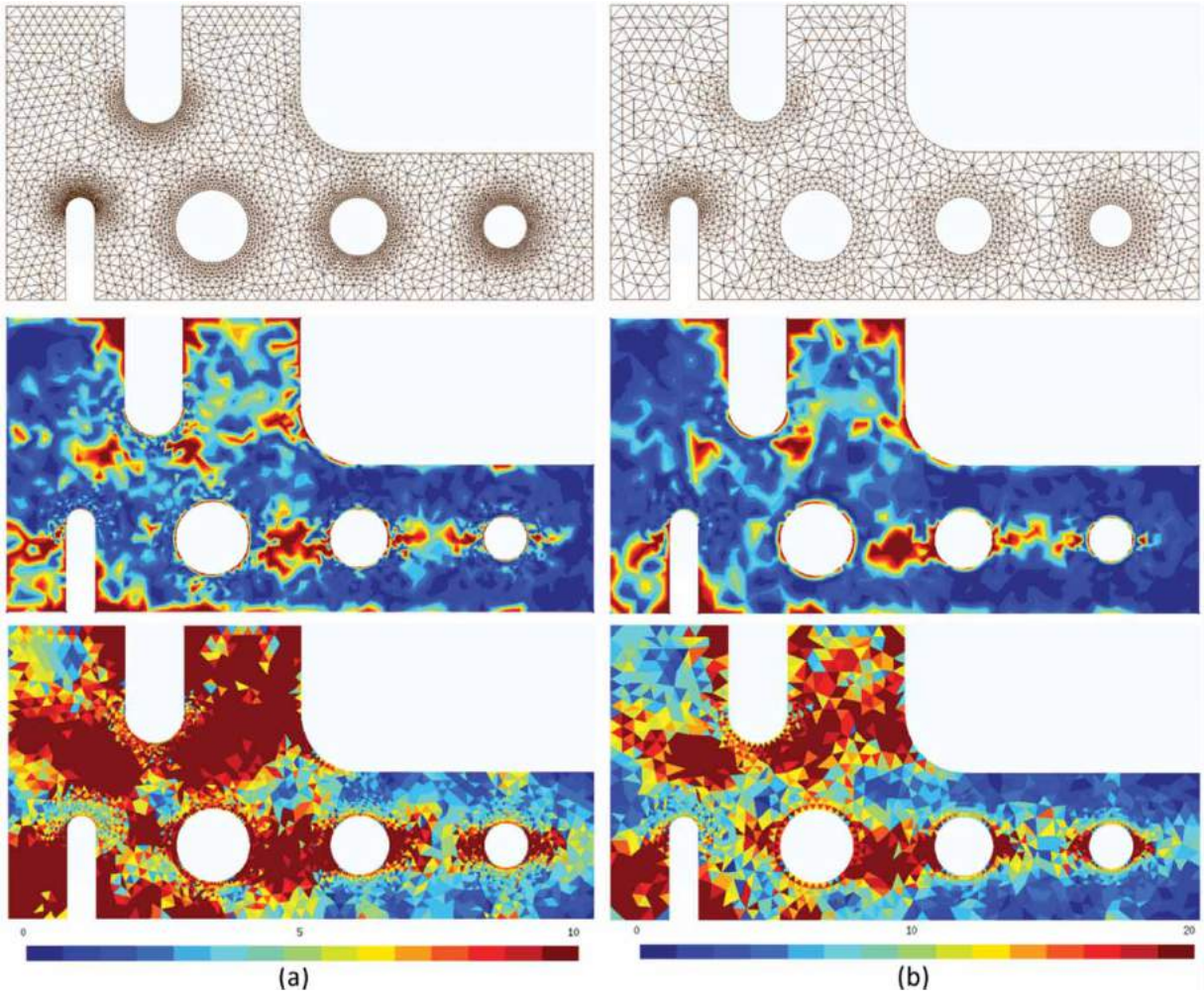

Figure 15. Results for the first case with multiple features (a) $\delta_{\text{target}} = 10\%$ (b) $\delta_{\text{target}} = 20\%$.

Table 4. Synthesis of results for the first case with multiple features.

Feature number	$\tilde{\sigma}_{VM}(x_c, y_c)$	$\delta(x_c, y_c)$ $\delta_{\text{target}} = 3\%$	$\delta(x_c, y_c)$ $\delta_{\text{target}} = 5\%$	$\delta(x_c, y_c)$ $\delta_{\text{target}} = 10\%$	$\delta(x_c, y_c)$ $\delta_{\text{target}} = 15\%$	$\delta(x_c, y_c)$ $\delta_{\text{target}} = 20\%$	$\delta(x_c, y_c)$ $\delta_{\text{target}} = 25\%$
1	*17.1 Pa*	*3,6%*	*4,7%*	*8,3%*	*11,5%*	*15,1%*	*17,6%*
2	*7,6 Pa*	*4,2%*	*6,1%*	*10,7%*	*14,3%*	*19,1%*	*22,8%*
3	*1,9 Pa*	*2,6%*	*4,7%*	*9,1%*	*13,3%*	*16,0%*	*19,4%*
4	*4,9 Pa*	*4,5%*	*6,1%*	*10,9%*	*16,0%*	*19,3%*	*22,8%*
5	*3,3 Pa*	*3,3%*	*5,0%*	*8,9%*	*12,8%*	*16,0%*	*19,1%*
6	*3,4 Pa*	*3,8%*	*5,6%*	*9,4%*	*13,0%*	*16,1%*	*19,0%*

closer to that used for reference von Mises stress distribution, and that consequently the unavoidable difference between reference von Mises stress distribution and the exact distribution has proportionally a higher impact.

3.4.2. Feature interference and side effects

Interference between features and side effects are part of the major problems that can be faced with the approach proposed in this paper and with a priori mesh adaptation in general. For all cases presented above, FEA results around a given feature are neither influenced by other neighboring features nor by vicinity with boundaries. In Fig. 16 the geometry of the previous validation case is modified to illustrate these effects. The location of two holes (holes 4 and 5) is changed so that hole 4 is closer to notches 1 and 2 and so that hole 5 is closer to the boundary. Reference von Mises stress distribution $\tilde{\sigma}_{VM}(x, y)$ and the FEA model are shown in Fig. 17. Note that the same color scale has been used for Fig. 14 and Fig. 17 for comparison and that the reference stress distribution well illustrates the interference between hole 4 and notches 1 and 2 and the side effect for hole 5.

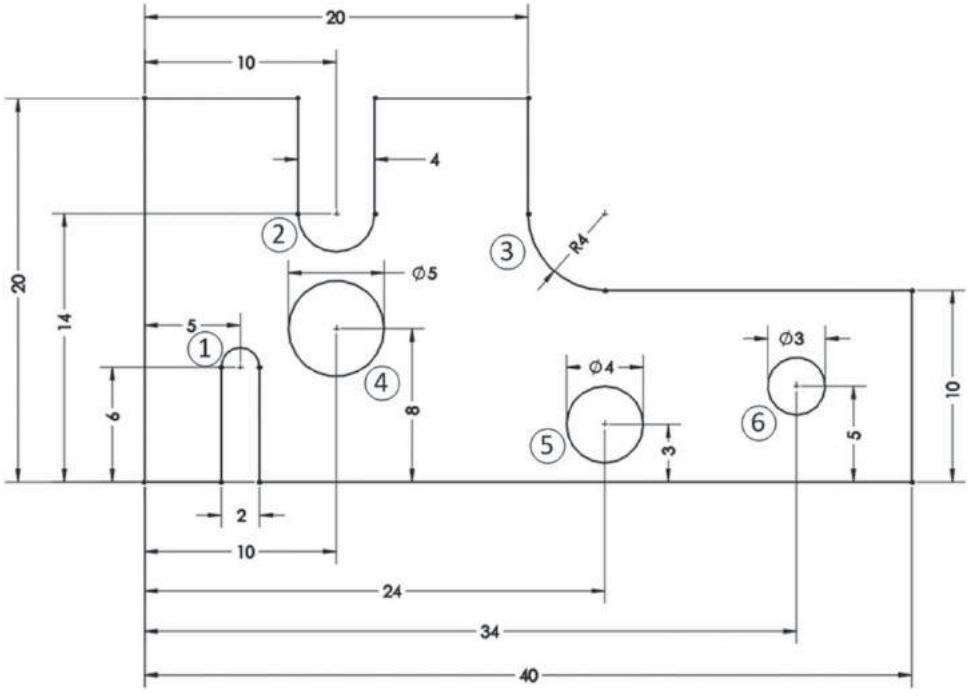

Figure 16. Geometry for the second case with multiple features.

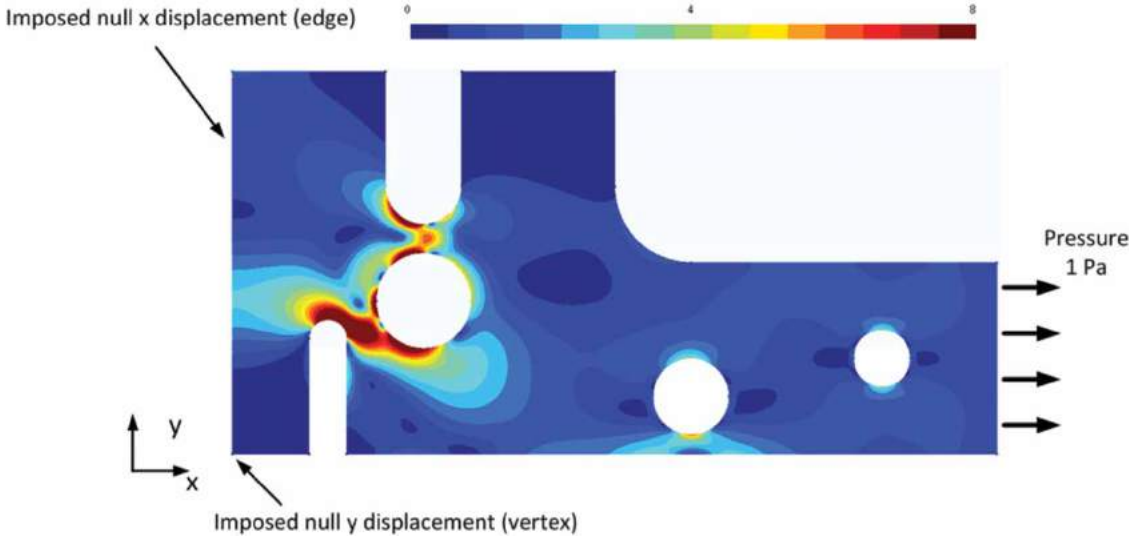

Figure 17. FEA model and reference von Mises stress $\tilde{\sigma}_{VM}(x, y)$ for the second case with multiple features.

Fig. 18a and Fig. 18b show meshes generated using the adaptation scheme proposed in this paper for respectively $\delta_{\text{target}} = 10\%$ and $\delta_{\text{target}} = 20\%$ and distributions of actual (middle figures) and estimated (lower figures) FEA errors $\delta(x, y)$ and $\delta_{ZZ}(x, y)$for these two accuracy objectives.

The synthesis of results in Tab. 5 first shows that, as expected, the maximum reference von Mises stress $\tilde{\sigma}_{VM}(x, y)$ increases for features 1,2,4 and 5 since stress distribution around these four features is clearly affected by changes made to the geometry. These results confirm that results globally tend to be worse for lower accuracy objectives.

However, these results also clearly illustrate that results are strongly and negatively affected by feature interference and side effects. Indeed, several results for features 2,4, and 5 show differences with accuracy objectives that are over 40% (in bold underlined while for results in red the objective is exceeded by 10%). This does not call into question the whole methodology but they enlighten that achieving better results in the case of feature interference and side effects would require further processing. A simple, but approximate, approach to decreasing $\delta(x_c, y_c)$ would be to apply a factor γ (with $\gamma < 1$) to coefficient α in equation 2 to features that are subject to feature interference and side effects.

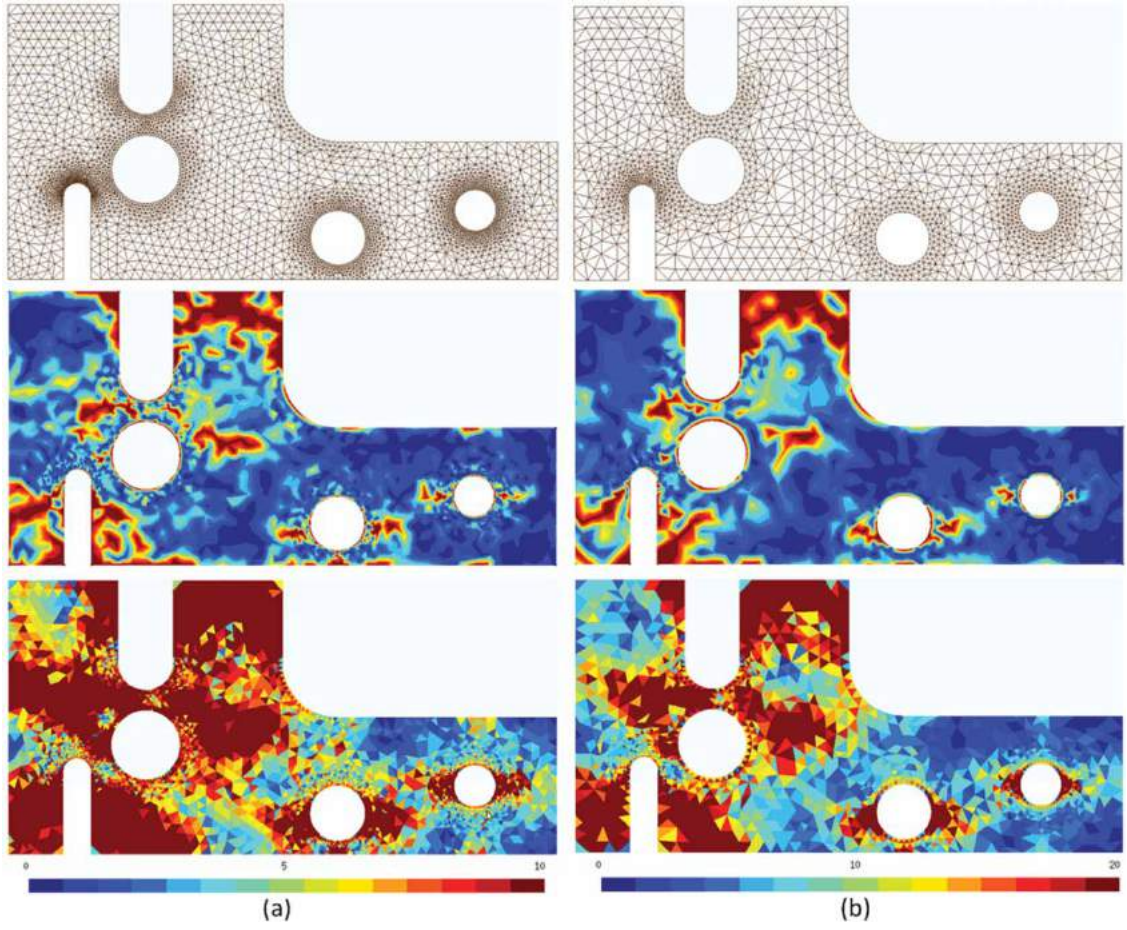

Figure 18. Results for the second case with multiple features (a) $\delta_{\text{target}} = 10\%$ (b) $\delta_{\text{target}} = 20\%$.

Table 5. Synthesis of results for the second case with multiple features.

Feature Number	$\tilde{\sigma}_{VM}(x_c, y_c)$	$\delta(x_c, y_c)$	$\delta(x_c, y_c)$ $\delta_{\text{target}} = 5\%$	$\delta(x_c, y_c)$ $\delta_{\text{target}} = 10\%$	$\delta(x_c, y_c)$ $\delta_{\text{target}} = 15\%$	$\delta(x_c, y_c)$ $\delta_{\text{target}} = 20\%$	$\delta(x_c, y_c)$ $\delta_{\text{target}} = 25\%$
1	*28.8 Pa*	*3,3%*	*5,3%*	*10,3%*	*14,3%*	*21,0%*	*22,0%*
2	*12,4 Pa*	***6,3%***	***9,6%***	***15,9%***	***22,8%***	***28,4%***	*33,9%*
3	*1,4 Pa*	*3,4%*	*5,5%*	*9,9%*	*14,3%*	*17,8%*	*21,2%*
4	*12,8 Pa*	***5,8%***	***9,0%***	***16,9%***	***23,0%***	***30,1%***	*33,5%*
5	*6,21 Pa*	***5,3%***	***7,5%***	***14,7%***	*18,4%*	*23,6%*	*27,3%*
6	*3,4 Pa*	*3,8%*	*5,6%*	*9,4%*	*13,0%*	*16,2%*	*19,1%*

This would first require detecting feature interference and side effects, based on distance between features (for feature interference) and distance between holes and the boundary (for side effects). Then, it is obvious that factor γ should decrease as distance between features and distance with the boundary decrease. However, using this approach would minimize the problem only and would not guarantee quantitative results for $\delta(x_c, y_c)$. A further approach to solving problems due to feature interference and side effects would be using a similar approach to the one used for single features, which means applying the approach to reference cases with two features and do a quantitative study of the effect of distance between these two features on $\delta(x_c, y_c)$.

4. Conclusion

The proposed methodology shows that quantitative results can be achieved in a priori mesh adaptation, which brings about interesting perspective with respect to the practical use of FEA, especially in early design stages along product development processes. It is a first step towards quantitative mesh pre-optimization and improvements can be foreseen either for achieving better results or for extending its fields of application. Further research is namely necessary to take into account feature interference and side effects and to extend the method to other types of features (slotted holes of V notches for example). However, for any feature for which $\delta^{ref} = F(E)$ is linear, the same methodology can be successfully applied. Another potential extension of this work is extending it to 3D elasticity problems. Indeed, as shown in [5], the a priori adaptation method presented in this paper can only be applied to 3D problems for which thickness effects are negligible. For 3D elasticity problems in general, further investigations are necessary but the same methodology can be used. The extension of the approach to other types of physical problems (thermal, CFD, electromagnetics, etc.) also represents a natural subject of research.

Acknowledgment

This study was carried out as part of a project supported by the Natural Sciences and Engineering Research Council of Canada (NSERC) and UQTR foundation.

ORCID

Jean-Christophe Cuillière http://orcid.org/0000-0002-4520-7748
Vincent Francois http://orcid.org/0000-0003-4239-6982

References

[1] Code Aster. Available: http://www.code-aster.org/
[2] OpenCascade. Available: http://www.opencascade.org/
[3] Babuska, I.; Melenk, J. M.: The partition of unity method, International Journal for Numerical Methods in Engineering, 40, 1997, 727–758.
[4] Belytschko, T.; Lu, Y. Y.; Gu, L.: Element-free Galerkin methods, International Journal for Numerical Methods in Engineering, 37(2), 1994, 229–256. http://dx.doi.org/10.1002/nme.1620370205
[5] Cuillière, J.-C.; François, V.; Lacroix, R.: A new approach to automatic and a priori mesh adaptation around circular holes for finite element analysis, Computer-Aided Design, 77, 2016, 18–45. http://dx.doi.org/10.1016/j.cad.2016.03.004
[6] Cuillière, J. C.; Francois, V.: Integration of CAD, FEA and Topology Optimization through a Unified Topological Model, Computer-Aided Design and Applications, 11(5), 2014, 1–15. http://dx.doi.org/10.1080/16864360.2014.902677
[7] Cuilliere, J. C.; Maranzana, R.: Automatic and a priori refinement of three-dimensional meshes based on recognition techniques, Advances in Engineering Software, 30, 1999, 139–149.
[8] Francois, V.; Cuilliere, J.-C.: An a priori adaptive 3D advancing front mesh generator integrated to solid modeling, Recent Advances in Integrated Design and Manufacturing in Mechanical Engineering, 2003, 337–346. http://dx.doi.org/10.1007/978-94-017-0161-7_33
[9] Francois, V.; Cuilliere, J. C.: Automatic mesh pre-optimization based on the geometric discretization error, Advances in Engineering Software, 31(10), 2000, 763–774. http://dx.doi.org/10.1016/S0965-9978(00)00057-0
[10] Geuzaine, C.; Remacle, J.-F.: Gmsh: a three-dimensional finite element mesh generator with built-in pre- and post-processing facilities, International Journal for Numerical Methods in Engineering, 79(11), 2009, 1309–1331. http://dx.doi.org/10.1002/nme.2579
[11] Grätsch, T.; Bathe, K. J.: A posteriori error estimation techniques in practical finite element analysis, Computers and Structures, 83(4–5), 2005, 235–265. http://dx.doi.org/10.1016/j.compstruc.2004.08.011
[12] Hughes, T. J. R.; Cottrell, J. A.; Bazilevs, Y.: Isogeometric analysis: CAD, finite elements, NURBS, exact geometry and mesh refinement, Computer Methods in Applied Mechanics and Engineering, 194(39–41), 2005, 4135–4195. http://dx.doi.org/10.1016/j.cma.2004.10.008
[13] Kang, E.; Haghighi, K.: Intelligent finite element mesh generation, Engineering with Computers, 11(2), 1995, 70–82. http://dx.doi.org/10.1007/BF01312201
[14] Kwok, W.; Haghighi, K.: A fuzzy logic knowledge-based approach for finite element mesh generation and analysis, Journal of Computing and Information Science in Engineering, 5(4), 2005, 317–329. http://dx.doi.org/10.1115/1.2052807
[15] Ladeveze, P.; Pelle, J. P.: Mastering Calculations in Linear and Nonlinear Mechanics, Springer, New York, 2004.
[16] Quadros, W. R.; Shimada, K.; Owen, S. J.: Skeleton-based computational method for the generation of a 3D finite element mesh sizing function, Engineering with

Computers, 20(3), 2004, 249–264. http://dx.doi.org/10.1007/s00366-004-0292-4

[17] Quadros, W. R.; Vyas, V.; Brewer, M.; Owen, S. J.; Shimada, K.: A computational framework for automating generation of sizing function in assembly meshing via disconnected skeletons, Engineering with Computers, 26(3), 2010, 231–247. http://dx.doi.org/10.1007/s00366-009-0164-z

[18] Takahashi, H.; Shimizu, H.: A general purpose automatic mesh generation using shape recognition technique, Proceedings of the International Conference on Computers in Engineering, 1, 1991, 519.

[19] Yagawa, G.; Yoshimura, S.; Nakao, K.: Automatic mesh generation of complex geometries based on fuzzy knowledge processing and computational geometry, Integrated Computer-Aided Engineering, 2(4), 1995, 265–280.

[20] Zienkiewicz, O. C.; Taylor, R. L.: The finite element method, volume 1 the basis, 2000, 689.

[21] Zienkiewicz, O. C.; Zhu, J. Z.: A simple error estimator and adaptive procedure for practical engineering analysis, International Journal for Numerical Methods in Engineering, 24(2), 1987, 337–357. http://dx.doi.org/10.1002/nme.1620240206

[22] Zienkiewicz, O. C.; Zhu, J. Z.: 'Accuracy and adaptivity in FE analysis: the changing face of practical computations,' in Computational Mechanics, 1991, pp. 3–12.